Journal of Experimental Botany, Vol. 76, No. 16 pp. 4640–4653, 2025
https://doi.org/10.1093/jxb/eraf215 Advance Access Publication 20 May 2025

RESEARCH PAPER

^{13}C labeling to determine intra-leaf photosynthetic heterogeneity dynamics during drought and rewatering

Junzhou Liu, Jinfang Zhao, Xiaoxia Ling, and Dongliang Xiong*

National Key Laboratory of Crop Genetic Improvement, Hubei Hongshan Laboratory, MARA Key Laboratory of Crop Ecophysiology and Farming System in the Middle Reaches of the Yangtze River, Huazhong Agricultural University, Wuhan 430070, China

* Correspondence: dlxiong@mail.hzau.edu.cn

Received 14 March 2025; Editorial decision 13 May 2025; Accepted 17 May 2025

Editor: Tracy Lawson, University of Illinois Urbana-Champaign, USA

Abstract

The spatial–temporal dynamics of photosynthetic heterogeneity within leaves under environmental fluctuations are still not well understood, limiting accurate assessments of plant photosynthetic capacity. Here, we combined $^{13}CO_2$ labeling with water status monitoring to quantify variations in intra-leaf photosynthetic rate (A_{13C}) during a drought–rewatering cycle. Hydraulic properties and anatomical traits were further investigated in well-watered plants. Under well-watered conditions, both A_{13C} and water use efficiency (WUE) increased progressively from the leaf base to the tip. However, severe drought followed by rewatering eliminated this longitudinal gradient in A_{13C}, with leaf tips exhibiting significantly impaired photosynthetic recovery. This impairment was associated with tip-specific limitations: (i) reduced water storage capacity exacerbating dehydration; and (ii) increased vulnerability of hydraulic conductance potentially leading to hydraulic failure. Importantly, the impaired leaf tips can result in reduced whole-leaf WUE. Our findings demonstrate the utility of $^{13}CO_2$ labeling for measuring leaf photosynthetic heterogeneity, reveal the dynamics of photosynthetic heterogeneity in response to environmental fluctuations, and highlight the vulnerability of leaf tips.

Keywords: $^{13}CO_2$, hydraulic capacitance, hydraulic vulnerability, isotope, leaf tip, maize, photosynthetic heterogeneity, rewatering, water use efficiency.

Introduction

Plants synthesize carbohydrates from CO_2 and water via photosynthesis, which is essential for their growth. Leaves are the primary organ for photosynthesis, but their photosynthetic rates vary, not only among different leaves within a canopy but also within distinct parts of the same leaf (Terashima, 1992). The variation in photosynthetic rate can be attributed to different environmental factors (Meinzer and Saliendra, 1997) and inherent differences in transcription, metabolism, and anatomical traits (Miranda *et al.*, 1981; Mayfield and Taylor, 1984; Long *et al.*, 1989; Zheng *et al.*, 2013; Ponnala *et al.*, 2014; Tausta *et al.*, 2014; AbdElgawad *et al.*, 2020; Strable and Nelissen, 2021). For experimental rigor and convenience, photosynthetic rates are typically assessed in specific leaf sections for comparative analyses across varieties or treatments. However, such localized measurements often fail to reflect the photosynthetic capacity at the canopy level (Medrano *et al.*, 2015; Fullana-Pericàs *et al.*, 2022; Chintala *et al.*, 2024). A deeper understanding of this photosynthetic heterogeneity can enhance the accuracy of measurements and modeling work at leaf or plant levels.

Crops belonging to the *Poaceae* family, characterized by their long and narrow leaves, exhibit longitudinal photosynthetic

heterogeneity. Many studies in maize, rice, sugarcane, and other *Poaceae* species have documented that photosynthetic capacity is lowest at the leaf base, progressively increasing towards the tip (Long *et al.*, 1989; Meinzer and Saliendra, 1997; Kodama *et al.*, 2011; Xiong *et al.*, 2015), occasionally with decreases at the tip (Repka and Jurekova, 1981; Ocheltree *et al.*, 2012; Verma *et al.*, 2020). In these studies, this spatial gradient is closely correlated with the non-uniform leaf structure and biochemistry for well-watered plants. However, crops in the field always face environmental fluctuations, with drought and rehydration being common scenarios. It remains unclear whether this spatial pattern of photosynthetic heterogeneity within the leaf is static or dynamic under changing environments. Given that the spatial stomatal heterogeneity may arise from heterogenous distribution of local hydraulic resistance (Nardini *et al.*, 2008), which is sensitive to drought, it is very likely that the photosynthetic heterogeneity within the leaf would change following drought (Pelleschi *et al.*, 2008; Verma *et al.*, 2020). In species with narrow and elongated blades, such as rice and some grasses, desiccation and tissue mortality primarily occur at leaf tips under high transpiration demand, soil drought, or excessive fertilizer conditions (Clary *et al.*, 2005; Ndjiondjop *et al.*, 2012; Pandey *et al.*, 2016; Riaz *et al.*, 2020), known as tip burn. Therefore, we hypothesize that the photosynthetic heterogeneity within the leaf would change after a drought–rewatering cycle due to the lower recovery capacity at leaf tips. Although internet searches for 'crop drought' often yield images showing tissue mortality starting at the leaf tip, mechanisms behind this phenomenon have not been well studied. Further research on this topic can enhance our understanding of plant carbon assimilation capacity under climate change.

Generally, post-drought photosynthetic recovery is influenced by two key factors, the stress level and the physiological recovery limitations. Firstly, despite most of the hydraulic resistance in leaves residing outside the xylem, water transport from the leaf base to the tip, coupled with the imbalance between water provision and loss, still results in a significant decline in water potential from the leaf base to the tip (Zwieniecki *et al.*, 2002; Cochard *et al.*, 2004b), leading to different stress levels during drought conditions. This impact may be amplified in long, narrow maize leaves. Secondly, stomatal limitation is the dominant constraint on post-drought photosynthetic recovery in maize, before lethal drought levels are reached (Liu *et al.*, 2024). The recovery of stomatal conductance post-drought may be constrained by various factors, such as hormone concentration and osmotic adjustment (Hasan *et al.*, 2024), particularly as a significantly reduced water transport capacity can inhibit leaf gas exchanges for an extended period (Skelton *et al.*, 2017; Rehschuh *et al.*, 2020; Wagner *et al.*, 2023). Therefore, we will focus on the heterogeneities in water status and hydraulic characteristics within the leaf to interpret the reduced recovery capacity at leaf tips.

Several methods have been developed to measure photosynthetic heterogeneity within leaves. One approach involves calculating changes in dry weight per unit leaf area before and after illumination of different leaf parts (Sestak and Bartos, 1962; Repka and Jurekova, 1981). However, this approach necessitates destructive sampling prior to illumination, potentially disrupting adjacent leaf gas exchange. Similarly, iodine staining has been utilized to identify photosynthetic starch accumulation across leaf segments (Harazono and Yabuki, 1982; Terashima *et al.*, 1988). Both methods suffer from the requirement for extended photosynthetic periods (hours), inevitably introducing errors due to photoassimilate transport. The introduction of portable gas exchange devices has significantly facilitated measurements of leaf gas exchange, emerging as a powerful tool in recent years for investigating photosynthetic heterogeneity (Lawson and Weyers, 1999; Ocheltree *et al.*, 2012; Li *et al.*, 2013; Xiong *et al.*, 2015; Zhang *et al.*, 2018; Yang *et al.*, 2023). Nevertheless, these instruments require sequential measurements of individual leaf parts, with each measurement requiring 5–10 min for stabilization (Ocheltree *et al.*, 2012). Additionally, the action of gripping leaves can significantly impact nearby leaf gas exchange (Buckley and Mott, 2001). Therefore, temporal disparities may introduce new errors. Furthermore, fluorescence detection and thermal imaging have been employed to characterize photosynthetic heterogeneity (Terashima, 1992; Song and Zhu, 2024), but accurately quantifying the photosynthetic rate remains a challenge (Edwards and Baker, 1993). Isotopes have great potential to evaluate photosynthetic heterogeneity. For instance, $^{14}CO_2$ (radioactive) labeling has been applied to characterize relative variations in photosynthesis within the leaf, but it similarly failed to provide precise measurements of the photosynthetic rate (Downton *et al.*, 1988; Wise *et al.*, 1992). In contrast, $^{13}CO_2$ (stable) labeling has proven useful in discriminating photosynthetic capacities in rice leaves under different water conditions (Wang *et al.*, 2023). By accurately controlling the $^{13}CO_2$ concentration, labeling duration, and environmental parameters, the application of $^{13}CO_2$ labeling coupled with tissue isotope abundance analysis is promising for quantifying photosynthetic rates across different leaf parts and eliminating errors stemming from differing measurement times.

In this study, we developed a $^{13}CO_2$ labeling method to quantitatively assess intra-leaf photosynthetic heterogeneity. We elucidated the fundamental principles and provided step-by-step operational protocols for this novel methodology. Employing this technique, we selected maize as our model organism to investigate intra-leaf photosynthetic heterogeneity. Two maize cultivars, Zhengdan 958 (ZD958) and Xianyu 335 (XY335), which are widely grown in China, were grown in pots for the experiment. We asked the following questions. (i) What are the temporal dynamics of this heterogeneity during a drought–rewatering cycle? (ii) How do varying water statuses and hydraulic properties influence the recovery of photosynthesis across different leaf sections?

Materials and methods

Plant materials and drought–rewatering treatment

The experiment was conducted in 2022 on the campus of Huazhong Agricultural University, located in Wuhan City, China. Maize seeds of two cultivars, Zhengdan 958 (ZD958) and Xianyu 335 (XY335), were sown in seed trays on 31 March. Then, three-leaf seedlings were transplanted to 18.9 liter pots filled with local clay soil [soil water-holding capacity, 38.9% (v/v); soil bulk density, 1.30 g cm^{-3}] 8 days after sowing (DAS). Ceramsite was spread over the bottom of the pot to act as a filtration layer. A fertilization schedule was applied to each pot, consisting of 1 g of compound fertilizer (containing 16% N, 16% P_2O_5, and 16% K_2O) and 0.5 g of urea dissolved in water, at weeks 1, 5, and 10 post-sowing. Plants were grown outdoors and regularly watered to avoid drought stress before treatment.

The drought–rewatering treatment commenced at the maize R2 stage, specifically 74 DAS. The vegetative growth almost stopped during this stage. For the well-watered group, plants received adequate watering at sunset each day, whereas for the drought–rewatering group, watering was withheld from the first day through the third day, then resumed at an adequate level in the afternoon of the fourth day and was maintained until the ninth day. Forty plants per cultivar were prepared for each treatment. Over the 9 d period, measurements were conducted at midday (11.00–14,00 h) on the first day to the fifth day and on the ninth day, including leaf water potential and intra-leaf heterogeneities of photosynthetic rate, osmotic potential, nitrogen content, and leaf mass per area. In addition, the intra-leaf heterogeneities of the pressure–volume (PV) curve, anatomy traits, and hydraulic vulnerability in well-watered plants were measured on 71–72, 80, and 88–89 DAS, respectively. All these traits were measured on leaves near the maize ear. The heterogeneity of traits within the leaf were evaluated by comparing the values at the tip with those at other positions.

Leaf water potential

Four plants from each cultivar and each treatment were randomly selected. One leaf per plant was sampled at midday (11.00–12.00 h) to measure the leaf water potential (Ψ_{leaf}, MPa) using a pressure chamber (3005, Soilmoisture Equipment Corp., USA). Prior to measurements, plastic film was wrapped around the sampled leaves for ~5 min to equilibrate.

Photosynthetic rate

After measuring the Ψ_{leaf}, the selected plants were subjected to measurement of the photosynthetic rate at midday (12.00–14.00 h). Leaves were positioned in a chamber containing $^{13}CO_2$ for a certain period of photosynthesis (Fig. 1A; Supplementary Fig. S1). Leaf regions with higher photosynthetic rates assimilate greater amounts of $^{13}CO_2$, leading to a higher detected ^{13}C abundance. Thus, the localized photosynthetic rate can be accurately determined by analyzing the ^{13}C abundance difference before and after labeling. The detailed operational procedure is as follows.

(i) To facilitate subsequent steps, each plant was trimmed to retain only one leaf near the ear. All other leaves and the stem tissue above this leaf were carefully removed.

(ii) The entire leaf was placed in a leaf chamber (length, 100 cm; width, 15 cm; height, 5 cm), and sealed with slime (gslime; Deli Group Co., China) to prevent leakage. The chamber was placed under light with the cover open for 30 min for photosynthetic induction. The photosynthetic photon flux density (PPFD) was ~1300 μmol m^{-2} s^{-1} at leaf height, close to the photosynthesis light saturation point for maize leaves, with an intensity ratio of ~13% purple, 13% blue, 23% green, 11% yellow, 7% orange, and 33% red. Room temperature was controlled at ~29 °C using an air conditioner, and relative humidity was maintained at ~60% with a humidifier. The device had four leaf chambers and thus can accommodate four plants for photosynthetic induction in a group.

(iii) The leaf chamber was first closed, and a mixed gas of 400 ppm $^{13}CO_2$, 80% N_2, and 20% O_2 at 60–70% relative humidity was injected into the leaf chamber. The flow rate of mixed air (80% N_2 and 20% O_2) was regulated at 10 l min^{-1} by a flow meter (YQB-731L-50; Provov, China); the flow rate of $^{13}CO_2$ was regulated at 4 ml min^{-1} by another flow meter (IKFD0-10SCCM; Beijing Ainuo, China). The appropriate amount of wet tissues was placed in the mixing box to maintain humidity. A mixing fan, operating at a wind speed of ~0.5 m s^{-1}, was positioned near the air intakes to ensure a uniform gas composition within the chamber. The airflow outside the chamber was filtered by NaOH solution to absorb the remaining $^{13}CO_2$.

(iv) After 2 min, the air injection was stopped, and subsequently the entire labeled leaf was sampled and stored under −20 °C. The next chamber was closed, and the operation was repeated to label the rest of the leaves. The lab was ventilated for 5 min between two labeling groups to avoid $^{13}CO_2$ pollution.

(v) The labeled leaf was evenly cut into eight segments from the tip to the base. Approximately 4 cm^2 of leaf tissue, avoiding the main vein, was sampled from each segment. After measuring the leaf area (a_{leaf}, cm^2), samples were dried in an oven to determine the DW (g). The leaf mass per area (LMA, g cm^{-2}) was calculated as DW divided by a_{leaf}.

(vi) Dry samples were ground into powder using a tissue grinder (Tissuelyser-32; Jingxin Co., Ltd., China).

(vii) Powdered leaf tissue samples of 1.5–2.0 mg were prepared for the measurement of carbon (C%, g g^{-1}) and nitrogen contents (mmol m^{-2}) and ^{13}C abundance ($\delta^{13}C$, ‰) using an elemental analyzer (Vario PYRO Cube, Elementar Trading Co., Germany) and a stable isotope ratio mass spectrometer (Isoprime 100, Elementar Trading Co., Germany). The proportion of ^{13}C to total C (R, dimensionless) was calculated by the following equation:

$$R = \frac{(\delta^{13}C/1000 + 1) \times 0.011237}{((\delta^{13}C/1000 + 1) \times 0.011237 + 1)} \quad (1)$$

The leaf localized photosynthetic rate based on the $^{13}CO_2$ labeling method (A_{13C}, μmol m^{-2} s^{-1}) was calculated by the following equation:

$$A_{13C} = \frac{DW \times C\% \times (R_{label} - R_{ref})}{a_{leaf} \times t \times m_c} \quad (2)$$

where R_{label} is the proportion of ^{13}C to total C in labeled samples; R_{ref} is the proportion of ^{13}C to total C in non-labeled samples, varying along the blade (see the Results); t is the equivalent assimilation time (s); and m_c is the molecular mass of the ^{13}C atom (13 g mol^{-1}).

During the labeling, the leaf chamber was primarily composed of $^{12}CO_2$ initially; the proportion of $^{13}CO_2$ progressively increased during the process of air injection. Therefore, it is crucial to note that t should not be 2 min during the calculation. Given the presence of a fan inside the chamber, the injected 400 ppm $^{13}CO_2$ was rapidly and continuously mixed with the internal air. Accordingly, we employed the integration method to calculate the equivalent assimilation time, which was determined to be 97.61 s (Supplementary Fig. S2).

Several tests were conducted to validate the reliability of the $^{13}CO_2$ labeling method in quantifying the photosynthetic rate.

Evaluating the carbon export during labeling

We measured the ^{13}C abundance at the labeled sites and nearby sites after 2 min labeling to evaluate the carbon export. Ten plants of ZD958 were used: five to evaluate the carbon export at the leaf tip (30% of leaf length from the ligule) and another five for the leaf base (70% of leaf length from the ligule). Labeling was conducted using a portable gas exchange device (Licor-6400; LI-COR, Inc., Lincoln, NE, USA). The air intake of the Licor-6400 was connected to mixed gas (800 ppm $^{13}CO_2$, 80% N_2,

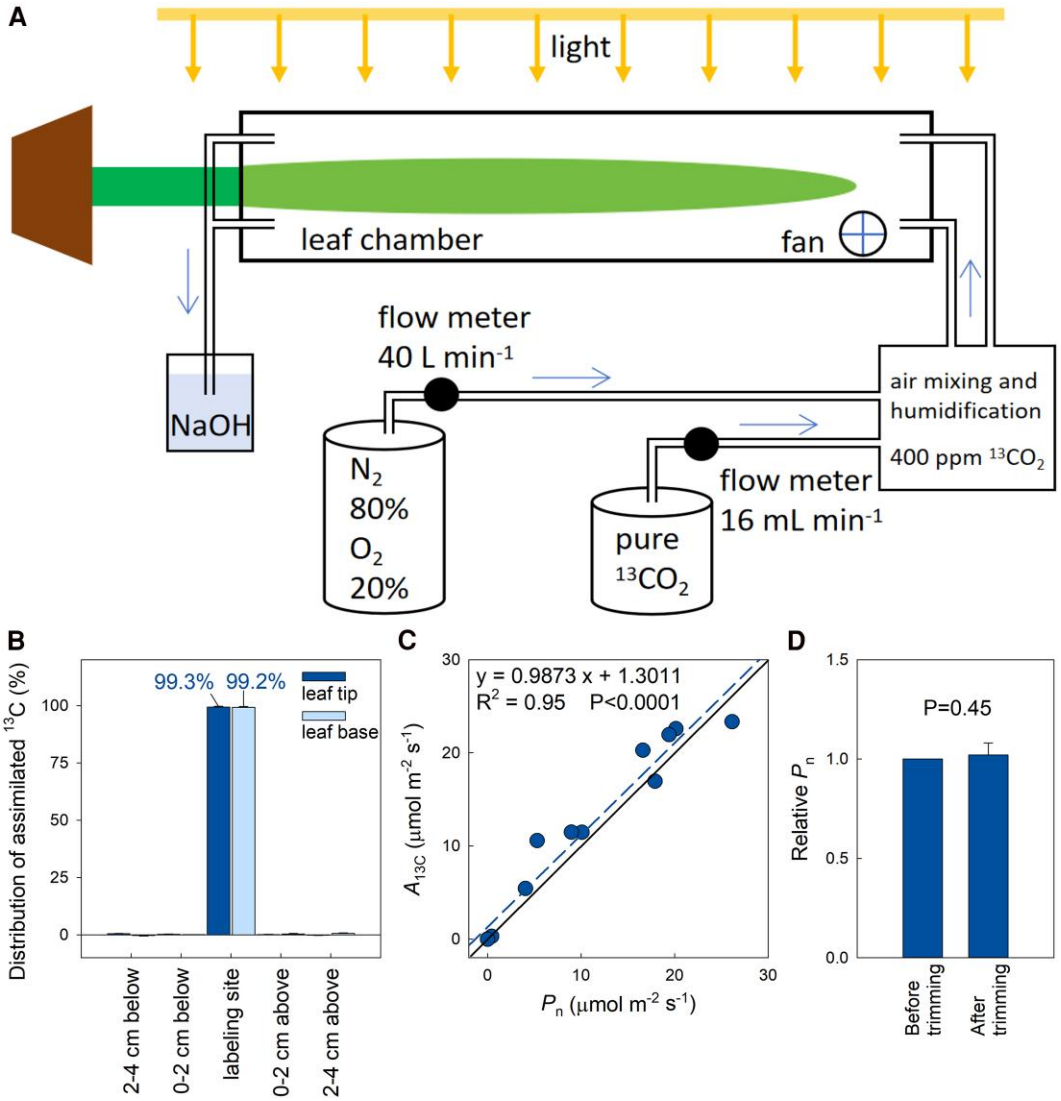

Fig. 1. The $^{13}CO_2$ labeling technique for measurement of the leaf photosynthetic rate. (A) Schematic diagram of the $^{13}CO_2$ labeling device. (B) Translocation of newly assimilated ^{13}C after a 2 min labeling. (C) Comparison of photosynthetic rate obtained using the $^{13}CO_2$ labeling technique (A_{13C}) and portable photosynthesis system (P_n). (D) Comparison of the photosynthetic rate measured before and after trimming. In (B) and (D) data are means ± SE, $n = 5$.

20% O_2; humidified to 50% relative humidity). In the leaf chamber, PPFD was set at 1300 μmol m^{-2} s^{-1} and air temperature was maintained at 25 °C. After 2 min of labeling using the leaf chamber, samples were collected from the labeled area and tissues located 0–2 cm and 2–4 cm above and below it to determine ^{13}C abundance according to the previous protocol. Prior to labeling, five control samples were collected from both the tip and the base sections to establish baseline ^{13}C abundance levels. Assimilated ^{13}C mass at the labeled site (M_{label}, g) and its proportion to the total (P_{label}, %) were calculated by the following equations:

$$M_{label} = DW \times C\% \times (R_{label} - R_{ref}) \quad (3)$$

$$P_{label} = \frac{M_{label}}{M_{-2} + M_{-1} + M_{label} + M_1 + M_2} \times 100\% \quad (4)$$

where M_{-2}, M_{-1}, M_1, and M_2 are assimilated ^{13}C mass at 2–4 cm and 0–2 cm below the labeled site and 0–2 cm and 2–4 cm above the labeled site, respectively. M_{-2}, M_{-1}, M_1, and M_2 were also calculated based on Equation 3.

Comparison between gas exchange and $^{13}CO_2$ labeling methods

Thirteen leaves from five plants of ZD958 were used in this comparison. Plants were desiccated to different drought levels. A portable gas exchange device (Licor-6800) was used to measure gas exchange at the middle section of each leaf. In the leaf chamber, PPFD was set at 1300 μmol m^{-2} s^{-1}, and air temperature, relative humidity, and CO_2 concentration were maintained at 27 °C, 60%, and 400 ppm, respectively. Results were recorded once the net photosynthetic rate (P_n, μmol m^{-2} s^{-1}) and stomatal conductance had stabilized. Subsequently, the air supply was immediately switched from ambient air to a mixed gas (400 ppm $^{13}CO_2$, 80% N_2, 30% O_2); temperature, light density, and relative humidity were maintained. After labeling for 2.5 min, the blade inside the leaf chamber was sampled to measure the ^{13}C abundance according to the previous protocol.

Impacts of trimming on P_n

In order to place the leaf for $^{13}CO_2$ labeling into the chamber and under the light, all other leaves and the upper stem section were removed. The P_n was measured before and 1 h after trimming in four plants of ZD958 using the Licor-6800.

Osmotic potential

After completing the $^{13}CO_2$ labeling process at step (v), leaf tissue samples were collected from three regions: the tip (the first and second segments from the apex), the middle (the fourth and fifth segments from the apex), and the base (the seventh and eighth segments from the apex). These samples were sealed in tubes and stored at −70 °C. The osmotic concentration of the sap extracted centrifugally from these samples was measured using a vapor pressure osmometer (VAPRO5600; Wescor Inc., Logan, UT, USA). The leaf osmotic potential (Ψ_{om}, MPa) was calculated employing the Van't Hoff equation based on the measured osmotic concentration; see Liu *et al.* (2024) for a detailed description.

Pressure–volume curves

Five well-watered plants from each cultivar were randomly selected. One leaf from each plant was harvested and rehydrated by submerging its cut end in water for 2 h to reach saturation (greater than −0.2 MPa). Samples were taken from the leaf tip (0–33% of the leaf length from the apex), middle (33–66% of the leaf length from the apex), and base (66–100% of the leaf length from the apex) positions to measure their PV curves. The PV curve was constructed by progressively drying the tissues on a laboratory bench while periodically measuring their water potential and mass. The water potential was measured using a pressure chamber (3005, Soilmoisture Equipment Corp., Goleta, CA, USA). The turgor loss water potential (Ψ_{tlp}, MPa), hydraulic capacitance before (C_{pre}, mmol m^{-2} MPa^{-1}) and after (C_{post}, mmol m^{-2} MPa^{-1}) Ψ_{tlp}, saturated water content (SWC, g H_2O g^{-1} dry mass), and other parameters were calculated according to the method of Sack and Pasquet-Kok (2011).

Generally, leaves measured for water potential in a pressure chamber require only their petioles to be open, with other parts remaining intact. However, to determine the PV curve and to follow leaf hydraulic conductance of different leaf parts, sampling various sections of the leaf for water potential measurement is necessary, inevitably resulting in two cut ends. Therefore, we conducted a preliminary experiment to determine the impact of two open cut ends and varying leaf lengths on water potential results. The results indicated that, as long as the maize leaf length exceeded 16 cm, the impact was negligible in this experiment (Supplementary Table S1).

Stomatal morphology

Five well-watered plants from each cultivar were randomly selected. Transparent nail polish was applied to the abaxial leaf surface at the tip, middle, and base sections. After drying, the nail polish was carefully peeled off and pasted onto a glass slide. An optical microscope (Ti-E; Nikon, Japan) was used to take photos of the stomatal footprints. Stomatal size (SS, μm^2) and density (SD, mm^{-2}) were analyzed using ImageJ software (National Institutes of Health, USA).

Leaf anatomies

Five well-watered plants from each cultivar were randomly selected. Samples were taken from the leaf tip, middle, and base sections for paraffin cross-sectioning. Standard paraffin sections were prepared and scanned by Wuhan Servicebio Technology Co., Ltd. Leaf thickness (LT, μm), vascular bundle density (VBD, mm^{-1}), distance from stoma to the nearest vessel (d_{s-v}, μm), vessel diameter (D_v), and $(t/b)^2$ (a parameter to characterize the structural strength of vessel cell walls; t, cell wall thickness; b, maximum span of vessel lumen) were analyzed using CaseViewer software (3DHISTECH Ltd., Hungary). Three replicates were randomly selected from each paraffin section for all these traits during measurements.

Notably, the calculation of VBD included both first-order (1°) and second-order (2°) veins. Considering the significant morphological differences between vein orders, measurements of D_v and $(t/b)^2$ were conducted on both orders.

Leaf hydraulic vulnerability

Leaf hydraulic vulnerability curves, which describe the leaf hydraulic conductance (k_{leaf}, mmol m^{-2} MPa^{-1} s^{-1}) change with water potential decline, were measured using the rehydration kinetics method (Brodribb and Holbrook, 2003). The remaining well-watered plants of ZD958 were desiccated to different drought levels, and leaves were sampled, wrapped in plastic film, and placed in the dark to achieve equilibrium. Following this, the water potential of the central portion of the leaf (Ψ_0, MPa) was measured. Then the leaf tip was excised under water and rehydrated for 20–30 s (t_r), after which its water potential (Ψ_f, MPa) was measured. k_{leaf} of the leaf tip was calculated as follows:

$$k_{leaf} = \frac{C \times \ln \frac{\Psi_0}{\Psi_f}}{t_r} \quad (5)$$

where C is hydraulic capacitance of the leaf tip determined from PV curves.

The k_{leaf} of the middle and base sections was measured using the same methodology.

The vulnerability curve was constructed by plotting k_{leaf} against Ψ_0, with regressions fitted using a sigmoidal function. The water potential inducing 50% loss of hydraulic conductance (P_{50}, MPa) was calculated accordingly.

Statistical analysis

The statistical software SPSS (IBM Corp., USA) was used to analyze the variance of the test data. One-way ANOVA or Student's t-test was performed to compare differences between treatments or leaf sections. Two-way ANOVA was performed to test for the effects of leaf section, time, and their interaction. The software SigmaPlot (Systat Software Inc., USA) was used to examine the correlations and prepare the figures.

Results

The reliability of the $^{13}CO_2$ labeling technology to measure photosynthetic rate

A $^{13}CO_2$ labeling method was developed to measure the leaf photosynthetic rate (Fig. 1A). To validate the reliability of this method, several experiments were conducted. First, we evaluated the transport of assimilates during labeling. When $^{13}CO_2$ labeling was applied for 2 min at one-third of the leaf length from the ligule, we observed that 99.3% of newly assimilated ^{13}C remained at the labeling site, with <0.7% potentially transported to the adjacent tissues (Fig. 1B). Similar results were found when labeling was conducted at two-thirds of the leaf length from the ligule. Second, we conducted a comparative analysis of the leaf photosynthetic rate measurements obtained from the same leaf middle position using a Licor-6800 or based on the principle of $^{13}CO_2$ labeling. The results demonstrated a strong correlation between the photosynthetic rates estimated

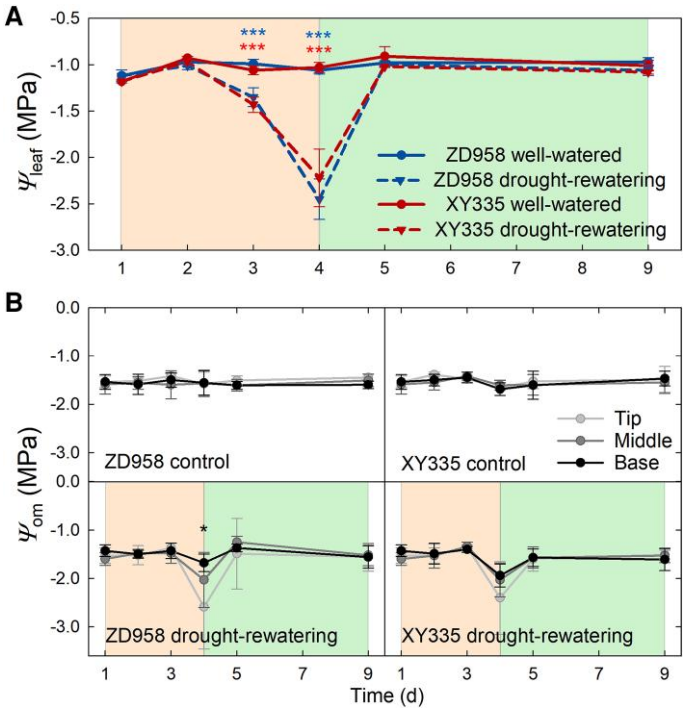

Fig. 2. Leaf potential dynamics. Dynamics of the (A) leaf water potential (Ψ_{leaf}) and (B) osmotic potential (Ψ_{om}) at midday during drought and rewatering. Data are means ± SE, $n = 4$. One-way ANOVA of treatment or position effects: $^{*}P < 0.05$; $^{***}P < 0.001$.

by two methods (Fig. 1C; $R^2 = 0.95$, $P < 0.0001$), with a slope of 0.987. Finally, we confirmed that tissue removal required for $^{13}CO_2$ labeling did not affect P_n (photosynthetic rate measured by Licor-6800; Fig. 1D).

Dynamic variations in intra-leaf heterogeneities in water status, photosynthetic rate, and C and N contents during a drought–rewatering cycle

Leaf water status

The drought–rewatering treatment induced severe drought stress on maize plants, significantly affecting their leaf water status. By the third day, both cultivars exhibited a significant decline in midday leaf water potential (Ψ_{leaf}) compared with the well-watered plants (Fig. 2A). On the fourth day, drought stress intensified, reducing Ψ_{leaf} further to −2.45 ± 0.22 MPa for ZD958 and −2.22 ± 0.31 MPa for XY335. Water supply was adequately restored that afternoon. By the fifth day, the second day after rewatering, Ψ_{leaf} quickly returned to pre-drought levels, exhibiting no significant difference from the well-watered plants.

The leaf osmotic potential (Ψ_{om}) at different positions within the leaf was monitored to evaluate its spatial variation (Fig. 2B). During the first 3 d, no significant differences in Ψ_{om} were observed between treatments for either cultivar. However, by the fourth day, severe drought led to a remarkable decrease in Ψ_{om}, particularly at the leaf tip of ZD958, where the decline was more pronounced compared with other

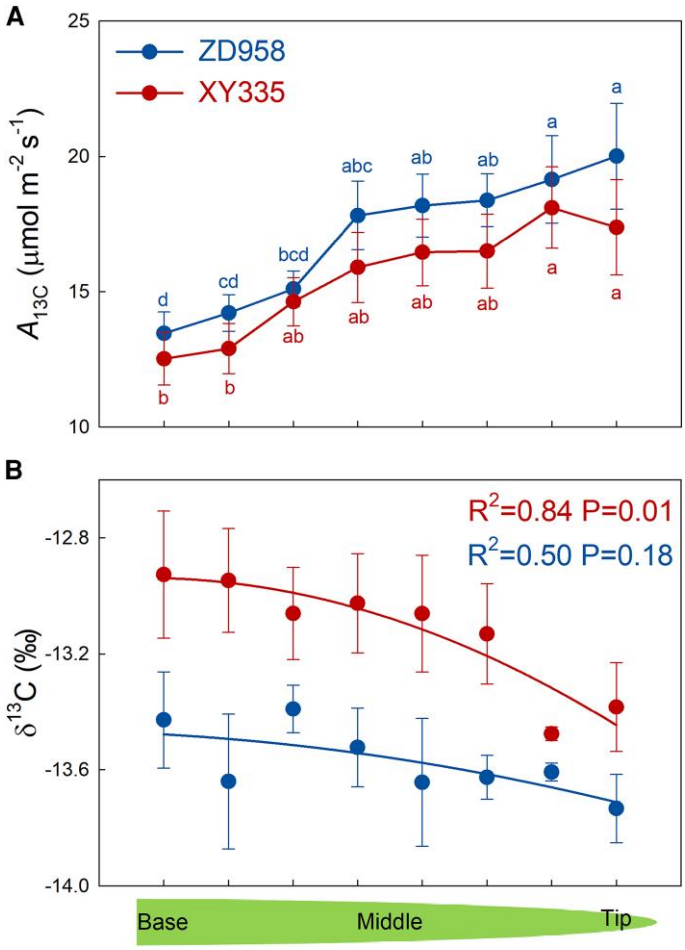

Fig. 3. Intra-leaf heterogeneities for well-watered plants. The intra-leaf heterogeneities of (A) photosynthetic rate and (B) ^{13}C abundance (unlabeled) for well-watered plants. A_{13C}, photosynthetic rate measured by the $^{13}CO_2$ labeling method. Results were the average values of well-watered plants measured on the first, fifth, and ninth days during the drought–rewatering cycle. Data are means ± SE. In (A), $n = 10$ for ZD958, $n = 12$ for XY335; in (B), $n = 3$. Different letters indicate significant differences among different leaf positions, as determined using one-way ANOVA followed by Duncan's test ($P < 0.05$).

leaf positions. Similar to the pattern observed in Ψ_{leaf}, Ψ_{om} recovered rapidly to pre-drought levels by the second day after rewatering. Notably, following the severe drought, dry leaf tips near the maize ear were observed in approximately a third of the plants (Supplementary Fig. S3). However, this condition was not clearly reflected in the measurements of Ψ_{leaf} and Ψ_{om}.

Photosynthetic rate measured by $^{13}CO_2$ labeling (A_{13C})

For well-watered plants of ZD958, the average A_{13C} during the drought and rewatering cycle displayed a significant increasing trend from the leaf base to the tip (Fig. 3), ranging from 13.5 ± 0.8 μmol m^{-2} s^{-1} to 20.0 ± 2.0 μmol m^{-2} s^{-1}. A similar pattern was observed in XY335.

For the treated plants, A_{13C} decreased across all leaf sections during the drought period, reaching 0 by the fourth day

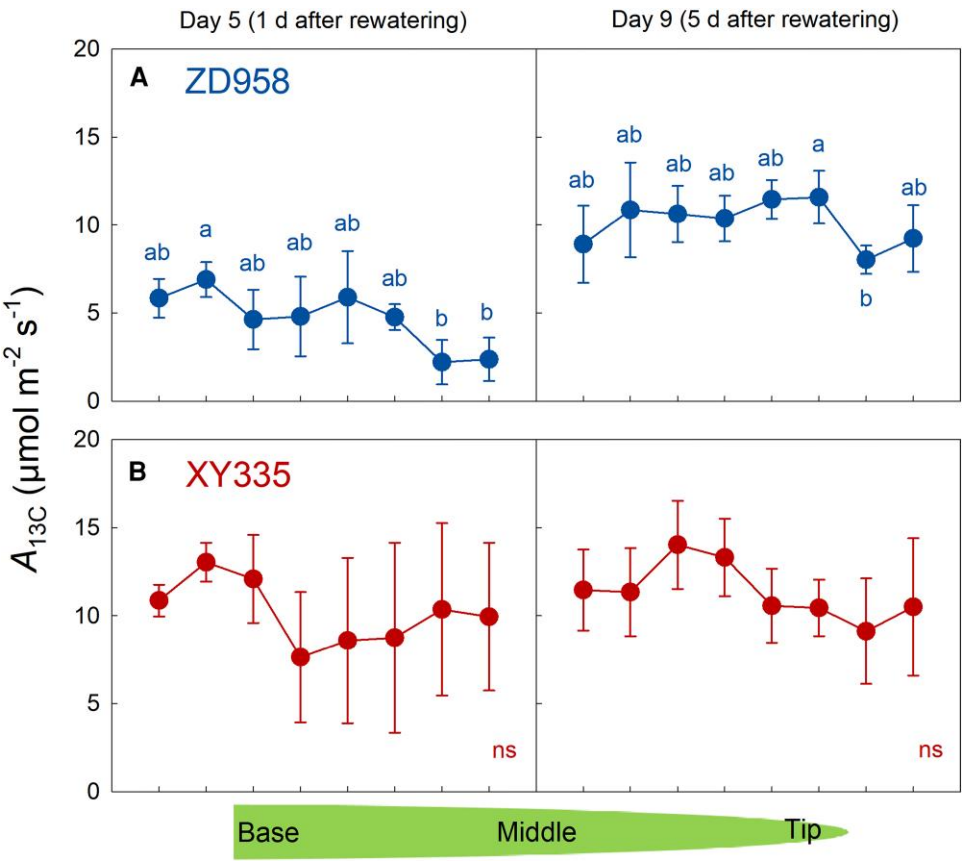

Fig. 4. Intra-leaf photosynthetic heterogeneity post-drought. The intra-leaf photosynthetic heterogeneity post-drought for (A) ZD958 and (B) XY335. A_{13C}, photosynthetic rate measured by the $^{13}CO_2$ labeling method. Data are means ± SE, $n = 4$. Different letters indicate significant differences among different leaf positions, and ns indicates no significant differences among them, determined using one-way ANOVA followed by Duncan's test ($P < 0.05$).

Table 1. Changes of photosynthetic heterogeneity and different photosynthetic recovery capacities within the maize leaf after drought and rewatering treatment

		Day	ZD958	XY335
Heterogeneity	A_{13C_tip}/A_{13C_mid}	1	1.10	1.17
		9	0.85	0.88
	A_{13C_tip}/A_{13C_base}	1	1.36	1.53
		9	1.04	0.92
Recovery ratio	Tip	9	50%	82%
	Middle	9	68%	95%
	Base	9	76%	120%

A_{13C}, the photosynthetic rate measured by $^{13}CO_2$ labeling technology; subscript tip, mid, or base are results measured at the leaf tip, middle, or base, respectively; recovery ratio, the ratio of A_{13C} in drought–rewatering-treated plants to that in well-watered plants; day 1, before the onset of drought; day 9, 5 d after rewatering.

(Supplementary Fig. S4). By the fifth day, the second day after rewatering, A_{13C} in ZD958 recovered to 2.2–6.9 μmol m^{-2} s^{-1}, with significantly higher values at the leaf base compared with the tip (Fig. 4). Although the leaf base of XY335 also showed higher A_{13C} than the tip, this difference was not significant. By the ninth day, although A_{13C} in ZD958 had further recovered, it remained significantly lower than that in well-watered plants (Supplementary Fig. S5). Specifically, the leaf tip recovered to only 50% of well-watered levels, while the middle and the base recovered to 68% and 76%, respectively (Table 1). In contrast, no significant differences in A_{13C} were observed between well-watered and treated plants of XY335, probably due to leaf senescence. However, recovery ratios for XY335 still varied, with the leaf base, middle, and tip reaching 120, 95, and 82% of well-watered levels, respectively.

Notably, after the drought–rewatering cycle, both cultivars exhibited minimal differences in A_{13C} along the leaf length, contrasting with the significant increase from the base to the tip in well-watered leaves. On the first day, A_{13C} at the leaf tip was 1.1–1.17 and 1.36–1.53 times that at the middle and base, respectively. However, following the drought–rewatering cycle, these ratios shifted to 0.85–0.88 and 0.92–1.04 (Table 1).

In addition, we observed that in unlabeled leaves, the abundance of ^{13}C ($\delta^{13}C$, ‰) gradually decreased from the base to the tip (Fig. 3B).

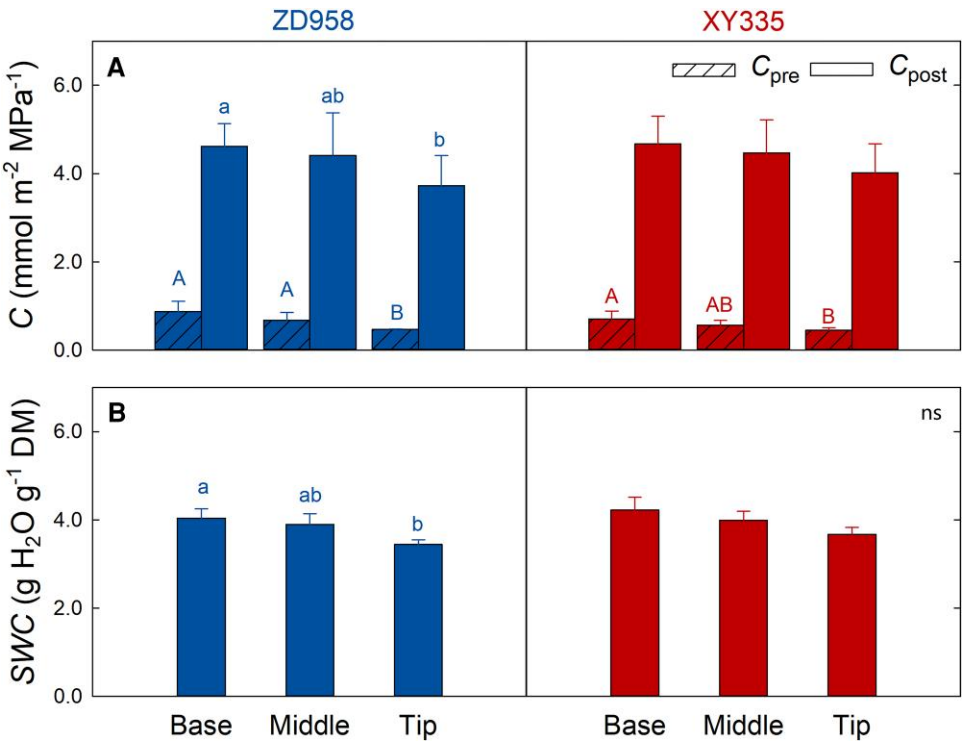

Fig. 5. Comparisons of leaf hydraulic capacitance and saturated water content. (A) Leaf hydraulic capacitance (*C*) and (B) saturated water content (SWC) between the leaf base, middle, and tip sections. C_{pre}, hydraulic capacitance before turgor loss; C_{post}, hydraulic capacitance after turgor loss; DM, dry matter. Data are means ± SE, $n = 5$. Different letters indicate significant differences among different leaf positions, as determined using one-way ANOVA followed by Duncan's test ($P < 0.05$).

Leaf mass per area

Prior to drought imposition, the LMA across leaf sections ranged from 45 g m^{-2} to 53 g m^{-2}, exhibiting a clear pattern with higher values concentrated in the central section and lower values at the two ends (Supplementary Fig. S6A). The application of drought–rewatering treatment significantly reduced the LMA of ZD958 leaves (Supplementary Table S2). In XY335, the effects of this treatment on LMA were limited, although it did cause a modest decline in some cases.

Leaf nitrogen contents

Prior to drought imposition, the leaf N content varied between 81 mmol m^{-2} and 108 mmol m^{-2} across leaf sections, showing a clear pattern with higher values concentrated in the central section and lower values at the two ends (Supplementary Fig. S6B). The drought–rewatering treatment induced a moderate decrease in N content in ZD958 leaves, with a statistically significant reduction confined to the central leaf region (Supplementary Table S2). In XY335, the impact of this treatment on leaf N content was limited.

Intra-leaf heterogeneities in pressure–volume, hydraulic, and morphology traits

Pressure–volume traits

We observed a significant decline in water storage capacity from the leaf base to the tip in well-watered plants. Specifically, the hydraulic capacitance pre-turgor loss (C_{pre}) at the leaf base was approximately twice that at the tip for both cultivars. Similarly, the hydraulic capacitance post-turgor loss (C_{post}) declined from the base to the tip, with this change being statistically significant in ZD958 (Fig. 5A). In addition, the SWC also displayed a significant reduction from the base to the tip in ZD958, while XY335 exhibited a similar decreasing trend, albeit not statistically significant (Fig. 5B). The water potential at turgor loss point, osmotic potential at full turgor, and modulus of elasticity did not change significantly across leaf sections for both cultivars (Supplementary Table S3).

Leaf hydraulic conductance and vulnerability

In ZD958, the k_{leaf} exhibited varying resistance to low water potential across different leaf sections (Fig. 6). The water potential inducing a 50% loss of k_{leaf} (P_{50}) gradually increased from the leaf tip (−1.19 MPa) to the base (−0.85 MPa). In contrast, the water potential inducing an 88% loss of k_{leaf} (P_{88}) significantly decreased from the leaf tip (−1.44 MPa) to the base (−2.00 MPa). Analysis of the vulnerability curves revealed an increasing trend in maximum k_{leaf} from the leaf tip to the base, with values ~17 mmol m^{-2} MPa^{-1} s^{-1} at the tip, 45 mmol m^{-2} MPa^{-1} s^{-1} at the middle, and >80 mmol m^{-2} MPa^{-1} s^{-1} at the base.

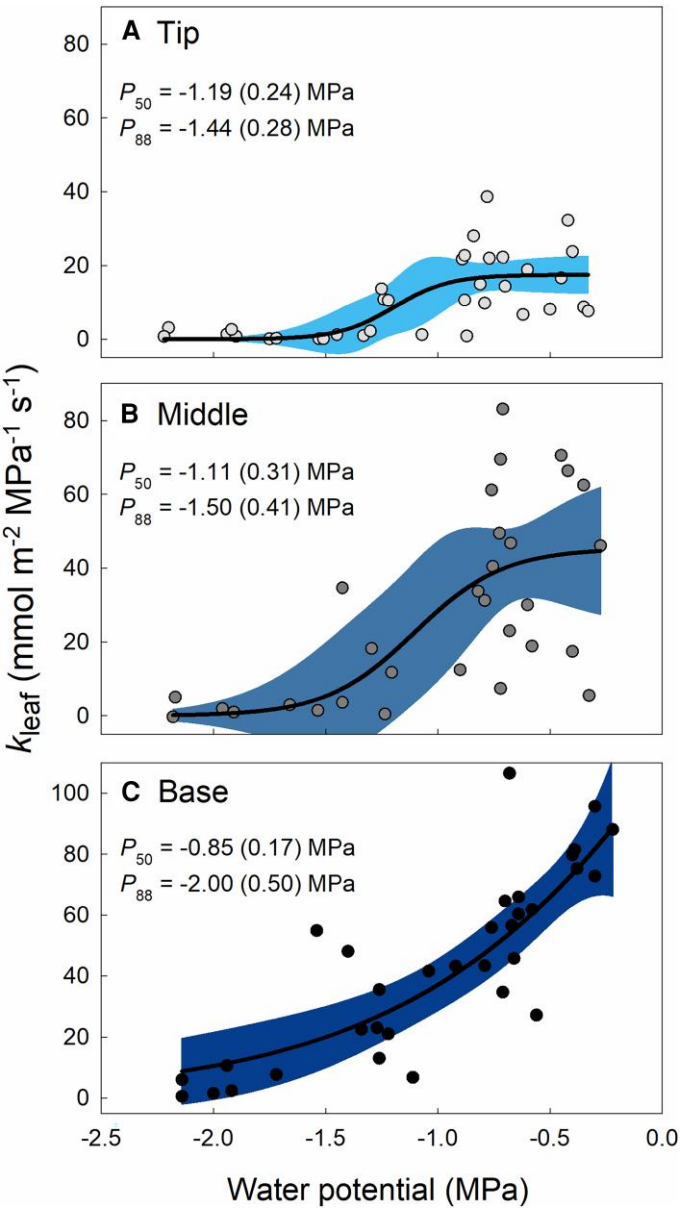

Fig. 6. Comparison of leaf hydraulic vulnerability of ZD958. A comparison of leaf hydraulic vulnerability between (A) the leaf tip, (B) middle, and (C) base sections of ZD958. k_{leaf}, leaf hydraulic conductance; P_{50} or P_{88}, the water potential inducing a 50% or 88% loss of k_{leaf}, respectively. The figure shows the original data points, the fitted curves, the 95% confidence bands, and means (95% confidence intervals) of P_{50} and P_{88}.

Stomatal morphology

SS and SD varied significantly along the leaf longitudinal axis (Table 2). For ZD958, leaf tips had the largest SS of 1345 ± 76 μm^2 and lowest SD of 145 ± 6 mm^{-2}, while the middle and base sections had a significantly smaller SS of ~1000 μm^2 and significantly higher SD of ~174 mm^{-2}. Similar trends were observed in XY335, but the SS in the middle was close to that in the tip and significantly larger than that in the base.

Leaf anatomies

LT, VBD, and d_{s-v} showed significant changes along the leaf longitudinal axis (Table 2). For ZD958, leaf tips had the smallest LT of 153 ± 5 μm and highest VBD of 8.3 ± 0.2 mm^{-1}, resulting in the shortest d_{s-v} of 74.1 ± 2.2 μm. In contrast, the middle and base sections had a significantly larger LT of ~186 μm, significantly lower VBD of ~7.0 mm^{-1}, and longer d_{s-v} of ~99 μm. Similar results were observed in XY335.

Vessels in 1° veins were much larger than those in 2° veins (Supplementary Fig. S7). In ZD958, the D_v significantly decreased from the leaf base to the tip, particularly in 1° veins, decreasing from 72.1 ± 2.3 μm at the base to 39.3 ± 0.6 μm at the tip (Table 2). The value of $(t/b)^2 \times 10^{-3}$ (a parameter to characterize the structural strength of vessel cell walls) in 1° veins significantly increased from 0.35 ± 0.02 at the base to 0.49 ± 0.04 at the tip. Conversely, $(t/b)^2$ in 2° veins significantly decreased from the base to the tip. Similar intra-leaf patterns were also found in XY335.

Discussion

^{13}C labeling enables reliable measurement of photosynthetic rate

Carbon isotopes have been used to identify photosynthetic heterogeneity within the leaf (Downton *et al.*, 1988; Wise *et al.*, 1992). Our study extends this understanding by quantitatively assessing photosynthetic rates along the length of maize leaves. The use of $^{13}CO_2$ labeling to determine photosynthetic rates rests on a solid theoretical foundation (Equation 2). Despite eventual distribution of assimilated ^{13}C to various plant organs, this transport effect is negligible within a short 2 min period (Fig. 1B). Consequently, the $^{13}CO_2$ labeling method and the portable gas exchange device can yield consistent rates of photosynthetic (Fig. 1C). Compared with the portable gas exchange device, the $^{13}CO_2$ labeling method offers two advantages. Firstly, it enhances measurement efficiency by maintaining a constant labeling duration (2 min), regardless of the number of measurement points within the leaf. In contrast, the portable gas exchange device requires 5–10 min per measurement point (Ocheltree *et al.*, 2012). Notably, our current setup allows for simultaneous light induction of four leaves, primarily constrained by the numbers of assimilation chambers and lights, which are cost-effective and can be scalable as needed. Secondly, the $^{13}CO_2$ labeling method eliminates temporal heterogeneity by ensuring simultaneous labeling of different leaf regions. These advantages become increasingly obvious with an increased number of intra-leaf measurement points. This method holds promise for quantifying photosynthesis heterogeneity at the canopy scale under field conditions, yet it faces some technical challenges, the primary one being how to efficiently replace ambient air with labeling gas in a large chamber within a short duration. If rapid mixing of chamber air can be achieved, this limitation could be addressed

Table 2. Comparisons of leaf anatomies and stomatal morphology between different positions within the maize leaf

Cultivar	ZD958			XY335		
Position	Base	Middle	Tip	Base	Middle	Tip
SS (μm^2)	948 ± 69 b	1076 ± 54 b	1345 ± 76 a	875 ± 22 b	1246 ± 88 a	1326 ± 63 a
SD (mm^{-2})	173 ± 7 a	175 ± 11 a	145 ± 6 b	172 ± 6 a	156 ± 4 a	134 ± 3 b
LT (μm)	184 ± 6 a	187 ± 9 a	153 ± 5 b	181 ± 8 a	184 ± 3 a	152 ± 0 b
VBD (mm^{-1})	6.8 ± 0.2 b	7.2 ± 0.2 b	8.3 ± 0.2 a	7.2 ± 0.1 b	7.6 ± 0.2 b	8.3 ± 0.2 a
ds–v (μm)	102.1 ± 4.6 a	95.4 ± 2.1 a	74.1 ± 2.2 b	101.5 ± 3.3 a	95.2 ± 1.8 a	72.3 ± 2.2 b
1° vein						
Dv (μm)	72.1 ± 2.3 a	55.0 ± 2.5 b	39.3 ± 0.6 c	69.8 ± 2.9 a	60.0 ± 2.2 b	45.8 ± 1.2 c
$(t/b)^2 \times 10^3$	0.35 ± 0.02 b	0.37 ± 0.04 b	0.49 ± 0.04 a	0.31 ± 0.02 b	0.31 ± 0.03 b	0.43 ± 0.03 a
2° vein						
Dv (μm)	12.6 ± 0.5 a	12.0 ± 0.4 ab	10.8 ± 0.5 b	14.4 ± 0.8	13.4 ± 0.6	12.6 ± 0.7
$(t/b)^2 \times 10^3$	3.27 ± 0.36 a	2.05 ± 0.18 b	2.15 ± 0.23 b	2.53 ± 0.19 a	1.59 ± 0.15 b	1.38 ± 0.10 b

SS, stomatal size; SD, stomatal density; LT, leaf thickness; VD, vein density; d_{s-v}, distance from stoma to the nearest vessel; D_v, vessel diameter; t/b, ratio of vessel cell wall thickness (t) to maximum span of the lumen (b). Data are means ± SE, $n = 5$. Different letters indicate significant differences between positions as determined by Student's t-test ($P < 0.05$).

through the application of an equivalent assimilation time in this study.

We think the A_{13C} measured using $^{13}CO_2$ labeling is different from the P_n of a portable gas exchange device. We all know that the net photosynthetic rate is obtained by subtracting respiration (including photorespiration and dark respiration) from the total. Firstly, synthesis and translocation of photosynthetic products require time, suggesting that dark respiration mainly uses non-recent photosynthates (Nogués *et al.*, 2004). Given our short labeling period, the fixed ^{13}C was not likely to have been used for dark respiration. Secondly, photorespiration occurs simultaneously with photosynthesis, sharing ribulose bisphosphate (RuBP) in reactions. The CO_2 released during photorespiration should be $^{12}CO_2$ in the short term, as the C atom in CO_2 comes from RuBP (Taiz and Zeiger, 2010). Subsequently, the $^{12}CO_2$ released during photorespiration was recycled for assimilation (Gerbaud and Andre, 1987; Delfine *et al.*, 1999). Additionally, the affinity of RuBP for $^{12}CO_2$ is substantially higher when compared with $^{13}CO_2$ (O'Leary, 1981; Gillon and Griffiths, 1997). Consequently, A_{13C} may reflect the RuBP carboxylation rate for $^{13}CO_2$, differing from P_n by a dark respiration rate.

The photosynthesis increased along the blade under well-watered conditions

Using the $^{13}CO_2$ labeling method, we observed an increasing trend in A_{13C} from the leaf base to the tip, with a slight decline potentially observable at the extreme tip (Fig. 3; Supplementary Fig. S4). This pattern is consistent with previous findings using portable gas exchange devices on maize and other *Poaceae* species (Long *et al.*, 1989; Meinzer and Saliendra, 1997; Xiong *et al.*, 2015).

The assessment of light and CO_2 response curves across different leaf sections indicated an increase in carboxylation rate from the base towards the tip (Long *et al.*, 1989), potentially underpinning photosynthetic heterogeneity within the leaf. Leaf N content, intimately tied to chlorophyll levels, governs carboxylation rates; however, in our study, variations in leaf N content did not align with A_{13C} values, peaking unexpectedly in the leaf middle section (Supplementary Fig. S6B). We speculate that the abundant N content throughout the leaf, due to our sufficient fertilization schedule, surpassed the threshold to limit photosynthesis (Paponov and Engels, 2003; Vos *et al.*, 2005), thereby negating a direct correlation. The enhanced carboxylation gradient along the leaf axis may introduce other photosynthetic limitations related to CO_2 transport rates (Long *et al.*, 1989). Consequently, leaf morphology must be adjusted to minimize CO_2 transport resistance. Despite the decreasing stomatal density from the leaf base to the tip, also observed by Zheng *et al.* (2013) and Miranda *et al.* (1981), the thinner leaf tissue and denser vascular bundles at the tip significantly shortened the distance between the stoma and the closest vessel (Table 2), thereby substantially reducing CO_2 resistance within the leaf (Kodama *et al.*, 2011; Ocheltree *et al.*, 2012). In addition, lower boundary layer conductance at the leaf tip may contribute to further decreasing CO_2 transport resistance (Harazono and Yabuki, 1982).

Leaf tips had the lowest photosynthetic recovery capacity after severe drought

After a severe drought and subsequent rewatering, the leaf tip exhibited the lowest photosynthetic recovery capacity compared with the middle and base sections (Fig. 4; Table 1), resulting in a significant change in photosynthetic heterogeneity within the leaf, supporting our hypothesis. Moreover, the severe drought

preferentially 'burned' the leaf tip (Supplementary Fig. S1), which aligns with the experience in agricultural practice (Ndjiondjop *et al.*, 2012; Pandey *et al.*, 2016; Franchetti and Pirri, 2022).

To interpret the lower photosynthetic recovery capacity at leaf tips, we analyzed the stress levels and hydraulic characteristics in different leaf sections. Water for leaf transpiration comes from the stem, thus the pathway to the leaf tip encounters the highest resistance. Furthermore, in maize and other *Poaceae* species, the leaf tip typically exhibits higher stomatal conductance and transpiration rate (Ocheltree *et al.*, 2012; Xiong *et al.*, 2015). Therefore, based on Ohm's law of sap flow (Van den Honert, 1948), the leaf tip should have the lowest water potential. Furthermore, our findings revealed that the leaf tip had the lowest saturated water content and hydraulic capacitance (Fig. 5), probably due to thinned blades (Table 2). Such limited water storage capacity may accelerate dehydration and water potential decline at the leaf tip during drought conditions. This is corroborated by our observation of a significant decline in Ψ_{om} at the leaf tip compared with other leaf positions on the fourth day of drought (Fig. 2B). This trend in Ψ_{om} under drought was also observed in a maize study (Michelena and Boyer, 1982). Given the weak osmotic adjustment capacity of maize leaves under drought (Erdei and Taleisnik, 1993; Liu *et al.*, 2024), the decline in osmotic potential at the leaf tip was attributed to dehydration, supported by a study that measured water potential along the maize leaf (Jain *et al.*, 2021).

Stomatal limitation is recognized as the primary determinant of photosynthetic recovery in maize leaves (Liu *et al.*, 2024). Significant damage to the maximum quantum yield of PSII associated with non-stomatal limitations has been documented only at extremely low RWC across various species (Trueba *et al.*, 2019; Wang *et al.*, 2023). In addition, despite the leaf N content significantly declining during the drought–rewatering cycle (Supplementary Fig. S6B), it remained adequate (Paponov and Engels, 2003; Vos *et al.*, 2005), unlikely to constrain photochemical processes. While maize leaf water status rapidly recovered from severe drought (Fig. 2), stomatal reopening may still be regulated by ethylene or residual abscisic acid (Bi *et al.*, 2023; Hasan *et al.*, 2024), and the ultimate stomatal conductance is largely influenced by hydraulic loss (Rehschuh *et al.*, 2020; Wagner *et al.*, 2023). Before rewatering, the average water potential of the entire leaf of ZD958 decreased to about −2.5 MPa (Fig. 2A). According to the leaf vulnerability curve (Fig. 6), the leaf tip may have lost most k_{leaf} during this period. In contrast, the base section may maintain a higher k_{leaf} due to potentially higher water potential and lower P_{88}. Notably, k_{leaf} consists of pathways both inside (k_x) and outside (k_{ox}) the xylem (Scoffoni *et al.*, 2023). Among them, the loss of k_x, induced by embolism, is difficult to repair (Johnson *et al.*, 2018). A previous study on maize leaf xylem vulnerability suggests an ∼40% loss of k_x under −2.5 MPa (Cochard, 2002), and this proportion may be even higher in leaf tips, resulting in greater limitations on gas exchange. Our findings are supported by a previous CT scanning study on maize leaves, which revealed that under drought conditions, embolism in veins initially occurred at leaf tips and edges (Ryu *et al.*, 2016).

The k_{leaf} and its vulnerability were correlated with vessel anatomical traits (Table 2). Specifically, the leaf base exhibited a larger maximum k_{leaf} compared with other sections, primarily attributed to its larger vessel size. Given the low P_{88} observed at the leaf base, the vessels in this region required enhanced structural strength to prevent cell wall collapse under high negative pressure (Cochard *et al.*, 2004a), thus exhibiting a higher $(t/b)^2$ value.

Conclusions and implications

The novel $^{13}CO_2$ labeling technique offers accurate measurements of photosynthetic heterogeneity within leaves. A_{13C} gradually increased from the maize leaf base to the tip under well-watered conditions. However, following a severe drought and subsequent rewatering, the leaf tip displayed the weakest photosynthetic recovery capacity, leading to dynamic changes in heterogeneity. This low photosynthetic recovery in the tip is attributed to more severe dehydration, lower water storage capacity, and more vulnerable hydraulics. Non-uniformly distributed light in the field may enhance the photosynthetic heterogeneity and exacerbate drought stress on leaf tips. As maize, rice, and wheat, major crops with similar leaf shapes and structures, belong to the *Poaceae* family, our findings have broad implications for crop physiology.

The photosynthetic recovery capacity of crops after drought represents their drought recovery. Generally, most previous studies only focused on a specific leaf position (Wang *et al.*, 2017; Johnson *et al.*, 2018; Song *et al.*, 2018). However, according to our conclusions, such photosynthetic recovery capacity could be overestimated (measured on the base or middle sections) or underestimated (measured on the tip section) at the leaf scale. In addition, old maize leaves at the bottom of the canopy seem to be more prone to senescence and mortality under drought (Supplementary Fig. S5), which can also affect the photosynthetic recovery capacity at the plant scale, but are often ignored. Hence, it is critical to holistically account for the photosynthetic heterogeneity within the canopy and its dynamic changes in future studies.

The decreasing trend in $\delta^{13}C$ values from the leaf base to the tip (Fig. 3B) indicates higher water use efficiency at the leaf tip than in other sections (Farquhar *et al.*, 1982; Twohey *et al.*, 2019). Similar results were also reported in other *Poaceae* crops (Meinzer and Saliendra, 1997; Kodama *et al.*, 2011). Considering that the damage to leaf tips initially after severe drought may significantly reduce the plant water use efficiency, exploring approaches to enhance drought tolerance of leaf tips is important and worth further investigation.

Supplementary data

The following supplementary data are available at *JXB* online.

Table S1. Effects of having two open cut ends and varying leaf lengths on pressure chamber-measured leaf water potentials.

Table S2. Significance levels of differences in LMA and N content between treated plants and well-watered plants.

Table S3. The changes of ψ_{tlp}, π_o, and ϵ between sections within the leaf.

Fig. S1. A photograph of the $^{13}CO_2$ labeling device during the experiment.

Fig. S2. Proportion of $^{13}CO_2$ to total CO_2 in the chamber during labeling.

Fig. S3. Photographs of maize plants after the drought–rewatering treatments.

Fig. S4. Changes of the photosynthetic rate of different positions within the leaf during a drought–rewatering circle.

Fig. S5. Significance analysis of the photosynthetic rate between different treatments on the ninth day.

Fig. S6. Dynamics of the leaf mass per area and leaf N content of different positions within the leaf during a drought–rewatering circle.

Fig. S7. Image of a maize leaf cross-section.

Acknowledgements

We acknowledge Jiahuan Liu for his assistance in designing the $^{13}CO_2$ labeling device and for his suggestions throughout the experiment; Sheng Liang, Kangkang Zheng, Yang Xiao, Enhui Xu, Xiaoxiao Wang, and Linna Zheng for their support in data collection; Dr Zhenmei Wang and Qiaoyun Zhang from the MARA Key Laboratory of Crop Ecophysiology and Farming Systems research platform in the Middle Reaches of the Yangtze River for their invaluable technical support and assistance throughout our experiments; and Limei Zhang, Qi Li, Ceng Yi, and Shu Zhu at the public laboratory platform of the College of Resources and Environment, Huazhong Agricultural University for their help with the tests of C and N contents and ^{13}C abundance.

Author contributions

JL and DX: conceptualization; JL, DX, and JZ: methodology; JL and XL: funding acquisition and visualization; JL and JZ: investigation; JL: writing—original draft; DX: project administration and supervision; XL and DX: writing—review & editing.

Conflict of interest

The authors have no conflicts to declare.

Funding

This research was supported by the National Natural Science Foundation of China (52209053) and the Key Research and Development Program of Hubei Province (2023BBB037).

Data availability

The primary data supporting this study were not made publicly available at the time of publication. The data that support the findings of this study are available from the corresponding author upon request.

References

AbdElgawad H, Avramova V, Baggerman G, *et al.* 2020. Starch biosynthesis contributes to the maintenance of photosynthesis and leaf growth under drought stress in maize. Plant, Cell & Environment **43**, 2254–2271.

Bi M-H, Jiang C, Brodribb T, Yang Y-J, Yao G-Q, Jiang H, Fang X-W. 2023. Ethylene constrains stomatal reopening in *Fraxinus chinensis* post moderate drought. Tree Physiology **43**, 883–892.

Brodribb TJ, Holbrook NM. 2003. Stomatal closure during leaf dehydration, correlation with other leaf physiological traits. Plant Physiology **132**, 2166–2173.

Buckley TN, Mott KA. 2001. Stomatal responses to non-local changes in PFD: evidence for long-distance hydraulic interactions. Plant, Cell & Environment **23**, 301–309.

Chintala S, Karimindla AR, Kambhammettu BP. 2024. Scaling relations between leaf and plant water use efficiencies in rainfed cotton. Agricultural Water Management **292**, 108680.

Clary J, SavÉ R, Biel C, De Herralde F. 2005. Water relations in competitive interactions of Mediterranean grasses and shrubs. Annals of Applied Biology **144**, 149–155.

Cochard H. 2002. Xylem embolism and drought-induced stomatal closure in maize. Planta **215**, 466–471.

Cochard H, Froux F, Mayr S, Coutand C. 2004a. Xylem wall collapse in water-stressed pine needles. Plant Physiology **134**, 401–408.

Cochard H, Nardini A, Coll L. 2004b. Hydraulic architecture of leaf blades: where is the main resistance? Plant, Cell & Environment **27**, 1257–1267.

Delfine S, Di Marco G, Loreto F. 1999. Estimation of photorespiratory carbon dioxide recycling during photosynthesis. Australian Journal of Plant Physiology **26**, 733–736.

Downton WJS, Loveys BR, Grant WJR. 1988. Non-uniform stomatal closure induced by water stress causes putative non-stomatal inhibition of photosynthesis. New Phytologist **110**, 503–509.

Edwards GE, Baker NR. 1993. Can CO_2 assimilation in maize leaves be predicted accurately from chlorophyll fluorescence analysis? Photosynthesis Research **37**, 89–102.

Erdei L, Taleisnik E. 1993. Changes in water relation parameters under osmotic and salt stresses in maize and sorghum. Physiologia Plantarum **89**, 381–387.

Farquhar GD, Oleary MH, Berry JA. 1982. On the relationship between carbon isotope discrimination and the intercellular carbon dioxide concentration in leaves. Australian Journal of Plant Physiology **9**, 121–137.

Franchetti B, Pirri F. 2022. Detection and localization of tip-burn on large lettuce canopies. Frontiers in Plant Science **13**, 874035.

Fullana-Pericàs M, Conesa MÀ, Gago J, Ribas-Carbó M, Galmés J. 2022. High-throughput phenotyping of a large tomato collection under water deficit: combining UAVs' remote sensing with conventional leaf-level physiologic and agronomic measurements. Agricultural Water Management **260**, 107283.

Gerbaud A, Andre M. 1987. An evaluation of the recycling in measurements of photorespiration. Plant Physiology **83**, 933–937.

Gillon JS, Griffiths H. 1997.The influence of (photo)respiration on carbon isotope discrimination in plants. Plant, Cell & Environment **70**, 1217–1230.

Harazono Y, Yabuki K. 1982. Studies on the effects of the leaf boundary layer resistance on the matter production of crop. (2) Distribution of the photosynthetic rate caused by the local difference in the boundary layer structures of individual leaves. Journal of Agricultural Meteorology **38**, 231–238.

Hasan MM, Liu X-D, Yao G-Q, Liu J, Fang X-W. 2024. Ethylene-mediated stomatal responses to dehydration and rehydration in seed plants. Journal of Experimental Botany **75**, 6719–6732.

Jain P, Liu W, Zhu S, *et al.* 2021. A minimally disruptive method for measuring water potential *in planta* using hydrogel nanoreporters. Proceedings of the National Academy of Sciences, USA **118**, e2008276118.

Johnson KM, Jordan GJ, Brodribb TJ. 2018. Wheat leaves embolized by water stress do not recover function upon rewatering. Plant, Cell & Environment **41**, 2704–2714.

Kodama N, Cousins A, Tu KP, Barbour MM. 2011. Spatial variation in photosynthetic CO_2 carbon and oxygen isotope discrimination along leaves of the monocot triticale (*Triticum* × *Secale*) relates to mesophyll conductance and the Peclet effect. Plant, Cell & Environment **34**, 1548–1562.

Lawson T, Weyers J. 1999. Spatial and temporal variation in gas exchange over the lower surface of *Phaseolus vulgaris* L. primary leaves. Journal of Experimental Botany **50**, 1381–1391.

Li S, Zhang Y-J, Sack L, Scoffoni C, Ishida A, Chen Y-J, Cao K-F. 2013. The heterogeneity and spatial patterning of structure and physiology across the leaf surface in giant leaves of *Alocasia macrorrhiza*. PLoS One **8**, e66016.

Liu J, Hochberg U, Ding R, Xiong D, Dai Z, Zhao Q, Chen J, Ji S, Kang S. 2024. Elevated CO_2 concentration increases maize growth under water deficit or soil salinity but with a higher risk of hydraulic failure. Journal of Experimental Botany **75**, 422–437.

Long SP, Bolharnordenkampf HR, Croft SL, Farage PK, Lechner E, Nugawela A. 1989. Analysis of spatial variation in CO_2 uptake within the intact leaf and its significance in interpreting the effects of environmental-stress on photosynthesis. Philosophical Transactions of the Royal Society B: Biological Sciences **323**, 385–395.

Mayfield SP, Taylor WC. 1984. The appearance of photosynthetic proteins in developing maize leaves. Planta **161**, 481–486.

Medrano H, Tomás M, Martorell S, Flexas J, Hernández E, Rosselló J, Pou A, Escalona J-M, Bota J. 2015. From leaf to whole-plant water use efficiency (WUE) in complex canopies: limitations of leaf WUE as a selection target. The Crop Journal **3**, 220–228.

Meinzer FC, Saliendra NZ. 1997. Spatial patterns of carbon isotope discrimination and allocation of photosynthetic activity in sugarcane leaves. Australian Journal of Plant Physiology **24**, 769–775.

Michelena VA, Boyer JS. 1982. Complete turgor maintenance at low water potentials in the elongating region of maize leaves. Plant Physiology **69**, 1145–1149.

Miranda V, Baker NR, Long SP. 1981. Anatomical variation along the length of the *Zea mays* leaf in relation to photosynthesis. New Phytologist **88**, 595–605.

Nardini A, Gortan E, Ramani M, Salleo S. 2008. Heterogeneity of gas exchange rates over the leaf surface in tobacco: an effect of hydraulic architecture? Plant, Cell & Environment **31**, 804–812.

Ndjiondjop MN, Futakuchi K, Cisse F, Baimey H, Bocco R. 2012. Field evaluation of rice genotypes from the two cultivated species (*Oryza sativa* L. and *Oryza glaberrima* Steud.) and their interspecifics for tolerance to drought. Crop Science **52**, 524–538.

Nogués S, Tcherkez G, Cornic G, Ghashghaie J. 2004. Respiratory carbon metabolism following illumination in intact French bean leaves using $^{13}C/^{12}C$ isotope labeling. Plant Physiology **136**, 3245–3254.

Ocheltree TW, Nippert JB, Prasad PVV. 2012. Changes in stomatal conductance along grass blades reflect changes in leaf structure. Plant, Cell & Environment **35**, 1040–1049.

O'Leary MH. 1981. Carbon isotope fractionation in plants. Phytochemistry **20**, 553–567.

Pandey V, Ansari MW, Tula S, *et al.* 2016. Dose-dependent response of *Trichoderma harzianum* in improving drought tolerance in rice genotypes. Planta **243**, 1251–1264.

Paponov IA, Engels C. 2003. Effect of nitrogen supply on leaf traits related to photosynthesis during grain filling in two maize genotypes with different N efficiency. Journal of Plant Nutrition and Soil Science **166**, 756–763.

Pelleschi S, Rocher JP, Prioul JL. 2008. Effect of water restriction on carbohydrate metabolism and photosynthesis in mature maize leaves. Plant, Cell & Environment **20**, 493–503.

Ponnala L, Wang Y, Sun Q, van Wijk KJ. 2014. Correlation of mRNA and protein abundance in the developing maize leaf. The Plant Journal **78**, 424–440.

Rehschuh R, Cecilia A, Zuber M, Faragó T, Baumbach T, Hartmann H, Jansen S, Mayr S, Ruehr N. 2020. Drought-induced xylem embolism limits the recovery of leaf gas exchange in Scots pine. Plant Physiology **184**, 852–864.

Repka J, Jurekova Z. 1981. Heterogeneity of the maize leaf blade in photosynthetic characteristics, respiration, mineral nutrient contents, and growth substances. Biologia Plantarum **23**, 145–155.

Riaz M, Mahmood R, Khan SN, Haider MS, Ramzan S. 2020. Onion tip burn: significance, and response to amount and form of nitrogen. Scientia Horticulturae **261**, 108773.

Ryu J, Hwang BG, Kim YX, Lee SJ. 2016. Direct observation of local xylem embolisms induced by soil drying in intact *Zea mays* leaves. Journal of Experimental Botany **67**, 2617–2626.

Sack L, Pasquet-Kok J, PrometheusWiki Contributors. 2011. Leaf pressure-volume curve parameters. http://prometheuswiki.org/tiki-index.php?page=Leaf%20pressure-volume%20curve%20parameters

Scoffoni C, Albuquerque C, Buckley TN, Sack L. 2023. The dynamic multi-functionality of leaf water transport outside the xylem. New Phytologist **239**, 2099–2107.

Sestak Z, Bartos J. 1962. Photosynthesis and chlorophyll content in different areas of fodder cabbage leaves. Biologia Plantarum **4**, 47–53.

Skelton RP, Brodribb TJ, McAdam SAM, Mitchell PJ. 2017. Gas exchange recovery following natural drought is rapid unless limited by loss of leaf hydraulic conductance: evidence from an evergreen woodland. New Phytologist **215**, 1399–1412.

Song H, Li Y, Zhou L, Xu Z, Zhou G. 2018. Maize leaf functional responses to drought episode and rewatering. Agricultural and Forest Meteorology **249**, 57–70.

Song Q, Zhu X-G. 2024. Techniques for photosynthesis phenomics: gas exchange, fluorescence, and reflectance spectrums. Crop and Environment **3**, 147–158.

Strable J, Nelissen H. 2021. The dynamics of maize leaf development: patterned to grow while growing a pattern. Current Opinion in Plant Biology **63**, 102038.

Taiz L, Zeiger E. 2010. Plant physiology. Sunderland, MA: Sinauer Associates, Inc.

Tausta SL, Li P, Si Y, Gandotra N, Liu P, Sun Q, Brutnell TP, Nelson T. 2014. Developmental dynamics of Kranz cell transcriptional specificity in maize leaf reveals early onset of C_4-related processes. Journal of Experimental Botany **65**, 3543–3555.

Terashima I, Wong SC, Osmond CB, Farquhar GD. 1988. Characterization of non-uniform photosynthesis induced by abscisic-acid in leaves having different mesophyll anatomies. Plant and Cell Physiology **29**, 385–394.

Terashima I. 1992. Anatomy of nonuniform leaf photosynthesis. Photosynthesis Research **31**, 195–212.

Trueba S, Pan R, Scoffoni C, John GP, Davis SD, Sack L. 2019. Thresholds for leaf damage due to dehydration: declines of hydraulic function, stomatal conductance and cellular integrity precede those for photochemistry. New Phytologist **223**, 134–149.

Twohey RJ, Roberts LM, Studer AJ. 2019. Leaf stable carbon isotope composition reflects transpiration efficiency in *Zea mays*. The Plant Journal **97**, 475–484.

Van den Honert TH. 1948. Water transport in plants as a catenary process. Discussions of the Faraday Society **3**, 146–153.

Verma KK, Song X-P, Zeng Y, Li D-M, Guo D-J, Rajput VD, Chen G-L, Barakhov A, Minkina TM, Li Y-R. 2020. Characteristics of leaf stomata and their relationship with photosynthesis in *Saccharum officinarum* under drought and silicon application. ACS Omega **5**, 24145–24153.

Vos J, van der Putten PEL, Birch CJ. 2005. Effect of nitrogen supply on leaf appearance, leaf growth, leaf nitrogen economy and photosynthetic capacity in maize (*Zea mays* L.). Field Crops Research **93**, 64–73.

Wagner Y, Volkov M, Nadal-Sala D, Ruehr NK, Hochberg U, Klein T. 2023. Relationships between xylem embolism and tree functioning during drought, recovery, and recurring drought in Aleppo pine. Physiologia Plantarum **175**, e13995.

Wang N, Gao J, Zhang S. 2017. Overcompensation or limitation to photosynthesis and root hydraulic conductance altered by rehydration in seedlings of sorghum and maize. The Crop Journal **5**, 337–344.

Wang X, Huang J, Peng S, Xiong D. 2023. Leaf rolling precedes stomatal closure in rice (*Oryza sativa*) under drought conditions. Journal of Experimental Botany **74**, 6650–6661.

Wise RR, Ortizlopez A, Ort DR. 1992. Spatial-distribution of photosynthesis during drought in field-grown and acclimated and nonacclimated growth chamber-grown cotton. Plant Physiology **100**, 26–32.

Xiong D, Yu T, Liu X, Li Y, Peng S, Huang J. 2015. Heterogeneity of photosynthesis within leaves is associated with alteration of leaf structural features and leaf N content per leaf area in rice. Functional Plant Biology **42**, 687–696.

Yang C, Zhou Q, Liu J, Liao J, Li R. 2023. Spatial variation characteristics of leaf light response during the grain filling period of summer maize in North China. Journal of Tianjin Agricultural University **30**, 69–75.

Zhang Y, Han J, Lei Z, Meng H, Zhang Y. 2018. Heterogeneity of photosynthetic capacity in different parts of leaf induced by leaf cupping of pima cotton (*Gossypium barbadense*). Journal of Shihezi University (Natural Science) **36**, 437–442.

Zheng YP, Xu M, Hou RX, Shen RC, Qiu S, Ouyang Z. 2013. Effects of experimental warming on stomatal traits in leaves of maize (*Zea may* L.). Ecology and Evolution **3**, 3095–3111.

Zwieniecki MA, Melcher PJ, Boyce CK, Sack L, Holbrook NM. 2002. Hydraulic architecture of leaf venation in *Laurus nobilis* L. Plant, Cell & Environment **25**, 1445–1450.